Quantum Metrology with Limited Measurement Resources


Jason Saunders


A senior thesis submitted to the faculty of
Brigham Young University
in partial fulfillment of the requirements for the degree of

Bachelor of Science


Jean-Francois Van Huele, Advisor


Department of Physics and Astronomy

Brigham Young University

April 2021

ABSTRACT

Quantum Metrology with Limited Measurement Resources

Jason Saunders
Department of Physics and Astronomy, BYU
Bachelor of Science

Quantum resources, such as entanglement, can decrease the uncertainty of a measurement procedure beyond what is classically possible. This phenomenon is well described for systems with asymptotically many measurement resources by the Quantum Cramer-Rao Bound, but no general description exists for the regime of limited measurement resources. I address this problem by defining a Bayesian quantifier for uncertainty suitable for the regime of limited resources, and by developing a mathematical description for two parameter-estimation procedures: using qubit probes to estimate a rotation angle induced on them, and using a Mach-Zehnder interferometer to estimate a phase shift. I simulate the qubit metrology scheme in the regime of limited resources. I show that, in noiseless systems, entanglement between qubits always decreases the uncertainty of the estimation; however, the quantum advantage decreases as fewer qubits are used in the estimation. I also show that the presence of strong dephasing noise removes the quantum advantage completely, regardless of the number of qubits used.

# Contents

# List of Figures

# Chapter 1

# Background

## 1.1  Metrology: The Science of Parameter Estimation

Parameter estimation plays a central role in science. Anytime we ask a quantitative question, like "What is the temperature of the substance?", "When did the event happen?", or "Where is the system located?", we need to estimate the relevant parameter in order to answer our question. The more precise our estimation is, the more specific of a question we can answer. Improving our estimations has the potential to benefit scientific investigation across many fields. Metrology is precisely the study of parameter estimation and how to improve it. In this thesis, we will study the field of quantum metrology, which investigates how quantum resources, such as entanglement and non-classical states of light, can be used to improve estimations. Particularly, we will investigate how utilizing quantum resources can decrease the uncertainty of a parameter estimation.

The terms parameter estimation and measurement are often used interchangeably, so it is worth distinguishing between the two for the purposes of this work. A parameter estimation is the entire process of determining the value of some parameter of interest. This involves preparing probes, interacting them with the system of interest, measuring the probes, then taking the measurement

results and constructing an estimate for the parameter of interest. A measurement, then, is a step in the estimation procedure. It involves extracting the relevant information from the probes after they have interacted with the system. A parameter estimation may include any number of measurements.

## 1.2    The Quantum Advantage: How Quantum Resources Can Decrease Uncertainty

Quantum resources can efficiently perform classically challenging–or in some cases classically impossible–tasks. Some examples of these tasks include using quantum computers to solve specific problems orders of magnitude faster than classical computers, or using quantum cryptography to achieve unbreakable connections.

*Quantum resources* and *quantum advantages* are central to this work and the field of quantum information at large. Quantum mechanics describes phenomena with no classical parallel–some examples include superposition, tunneling, and entanglement, along with non-classical states of light. These phenomena are the keys which allow us to perform the aforementioned classically-challenging or classically-impossible tasks. When a quantum phenomenon is utilized in a task, we label it a quantum resource. The two quantum procedures described in this thesis use quantum entanglement and non-classical states of light as their quantum resources. In a similar vein, whenever a procedure utilizing quantum resources is able to outperform a similar classical procedure, we say that we have achieved a quantum advantage–the use of quantum resources has given us an advantage. As demonstrated by the Quantum Cramer-Rao Bound [1], we can achieve a quantum advantage in the field of metrology.

The Quantum Cramer-Rao Bound describes the lowest achievable uncertainty for an estimation procedure. It is a quantum extension of a classical result, the Cramer-Rao Bound [2]. The Quantum

Cramer-Rao Bound states

$$\delta\phi \geq \frac{1}{(\Delta h)(2\sqrt{\nu})}. \tag{1.1}$$

In this inequality, $\delta\phi$ is the uncertainty of $\phi$, the parameter we are estimating. The quantity $\Delta h$ is the variance of $h$, which is the generator of $\phi$. Think of $h$ as encoding the interaction which imprints $\phi$ onto our measurement probes. Finally, $\nu$ is the number of measurements we make in our estimation. The Quantum Cramer-Rao Bound assumes that the number of measurements $\nu$ is asymptotically large. In this regime, the Quantum Cramer-Rao Bound is tight, meaning that there exists some system which can reach the lower bound.

The Quantum Cramer-Rao Bound is exact only when $\nu$ is infinitely large. Although it is inexact when dealing with any finite value of $\nu$, the error becomes negligible as the number of measurements approaches infinity. We consider the number of measurements to be *asymptotically large* when the difference between the true lower bound and the lower bound predicted by the Quantum Cramer-Rao Bound is negligible. What is considered negligible depends on the level of precision required, so there is not a unique boundary between the asymptotic regime and its counter part, the limited or non-asymptotic regime. For this work, we define the *limited regime* as the area where results differ qualitatively from the asymptotic regime.

The Quantum Cramer-Rao Bound is a very general condition; it can be derived for specific systems by choosing the right generator $h$. In [3], this bound is derived for a more specific measurement procedure: $N$ identical probes per measurement. The lower bound of the uncertainty $\delta\phi_s$ is derived assuming that the $N$ probes are separable (uncorrelated), and the lower bound $\delta\phi_e$ is derived by assuming that all $N$ probes are maximally entangled together. Comparing the two bounds, the authors find

$$\delta\phi_e = \frac{\delta\phi_s}{\sqrt{N}}. \tag{1.2}$$

Apparently, for this class of systems, entanglement reduces the lower bound of the uncertainty by a

factor of $1/\sqrt{N}$ in the regime of asymptotically large $\nu$.

The Quantum Cramer-Rao Bound only holds when the number of measurements $\nu$ is asymptotically large. This covers a large space of possible measurement scenarios, but there exist other situations where the number of measurements is small and limited. Imagine that an estimation procedure is destructive, so a sample can only be measured a handful of times. Or perhaps the measurement target is in motion, and there is a limited time window available for measurement. In these cases, we want to understand how quantum resources can improve our estimation procedures. Is the benefit of entanglement the same in the limited regime as in the asymptotic regime? Is the quantum advantage larger, smaller, or perhaps nonexistent?

This non-asymptotic, or limited, regime has been studied before. Some analytical quantum bounds for the uncertainty have been proposed, such as the Ziv-Zakai bound [4] and the Weiss-Weinstein bound [5], but neither of these bounds are tight–we are not guaranteed to be able to reach their lower bounds [6]. Specific systems, such as interferometric estimation schemes, have also been investigated numerically in this regime [6], but the results do not extend to other estimation procedures.

The discussion thus far has assumed the absence of noise, but noise is an important factor to consider when designing real-world applications. In the asymptotic regime, it has been shown that the presence of even small amounts of some types of noise, such as dephasing, can completely wipe out the quantum advantage, although there is still a reduced quantum advantage in the presence of other types of noise [7]. It has also been shown that the quantum advantage can be salvaged if the number of measurements is kept small enough [8].

## 1.3 My Contribution: Quantum Metrology with Limited Resources

In this thesis, I study two specific estimation procedures in the non-asymptotic regime: estimating a rotation induced on qubit probes, and estimating a phase shift using a Mach-Zehnder interferometer. In Chapter 2, I use Bayesian methods to develop a measure of uncertainty which is applicable for regimes of very limited measurement information. I also develop the equations and transformations necessary to simulate the qubit and the Mach-Zehnder interferometer estimation protocols. Additionally, for the qubit system, I include the transformations necessary to simulate dephasing noise in the qubits. Results for the qubit simulations are presented in Chapter 3. I use a single class of states as probes to study the effect that entanglement between the qubits has on the uncertainty of the estimation. I also simulate dephasing noise, a type of decoherence, and determine how it affects the quantum advantage. I find that, in the noiseless simulations, entanglement provides a quantum advantage, although the advantage is smaller than in the asymptotic regime. The presence of weak dephasing noise reduces this quantum advantage, although entanglement still decreases the uncertainty of the estimation. Strong dephasing noise removes the quantum advantage entirely. Preliminary results for the Mach-Zehnder interferometer estimation protocol simulations are given in Appendix A.

This work deals only with single parameter estimation. Information about multi-parameter quantum metrology can be found in [9].

# Chapter 2

# Methods

## 2.1 Measurement and Parameter Estimation in the Regime of Limited Resources

### 2.1.1 Motivating a Bayesian Approach

Estimating a parameter with limited resources is challenging. Imagine first the following situation: we want to measure the angle of a magnetic field using many neutrally charged spin particles, initialized in the spin up position. We send the particles through the field, then measure each one individually, recording either spin up or spin down. From our measurement results we can reconstruct the wave function of the particles, from which we can estimate the angle of the magnetic field. We could further define an uncertainty of our estimation by repeating the procedure many times and recording the variation in the estimation result.

Now imagine this second situation: we again want to measure the angle of a magnetic field, but this time we have only a single neutrally charged spin particle. We initialize the particle in the spin up position and send it through the field. We measure it, recording either spin up or spin down.

From this single datapoint, what can we say about the angle of the magnetic field? We lack the information to reconstruct the wave function with any degree of certainty, and so would be hard pressed to come up with an angle of the field, or an uncertainty of our estimation, using the same methods as we used in the many particle case. So what can we say?

### 2.1.2   A Bayesian Quantification of the Uncertainty

Bayesian methods center on the idea of calculating the probability, or likelihood, of a hypothesis. Given our measurement results, whether they be a single data point or many, we can calculate the probability that the parameter of interest lies within a specific range. We can use Bayesian ideas to define an uncertainty metric for our limited-resources measurement procedures. To do this, we will first introduce some useful functions, then use them to quantify the uncertainty of a general parameter $\phi$ in the regime of non-asymptotic, limited $\nu$.

First we will define a complete, orthogonal measurement basis, comprised of states $|\xi_1\rangle, \ldots, |\xi_m\rangle$, where $m$ is the dimensionality of the probe. Let $\Xi_i(\phi)$ be the probability of measuring $|\xi_i\rangle$ if the initial state $|\psi\rangle$ has been transformed by the $\phi$-dependent evolution $U_\phi$

$$\Xi_i(\phi) = \left| \langle \xi_i | U_\phi(\phi) | \psi \rangle \right|^2. \tag{2.1}$$

Next, we'll define a function $P_{\{k\}}^\nu(\phi, \nu, k_1, k_2, \ldots, k_m)$, which is an unnormalized probability distribution as a function of the angle of rotation $\phi$, given that $|\xi_1\rangle$ was measured $k_1$ times, $|\xi_2\rangle$ $k_2$ times, and so on, for a total of $\nu$ measurements:

$$P_{\{k\}}^\nu(\phi, \nu, k_1, \ldots, k_m) = \frac{\nu!}{k_1! k_2! \cdots k_m!} \prod_{i=1}^m \Xi_i^{k_i}(\phi). \tag{2.2}$$

The fraction on the right-hand side of the equation is a combinatorial factor resulting from counting all the possible orderings of the $\nu$ measurements multiplied by the probability of measuring that specific set of measurements. Finally, we define a third function, a weighted, normalized probability
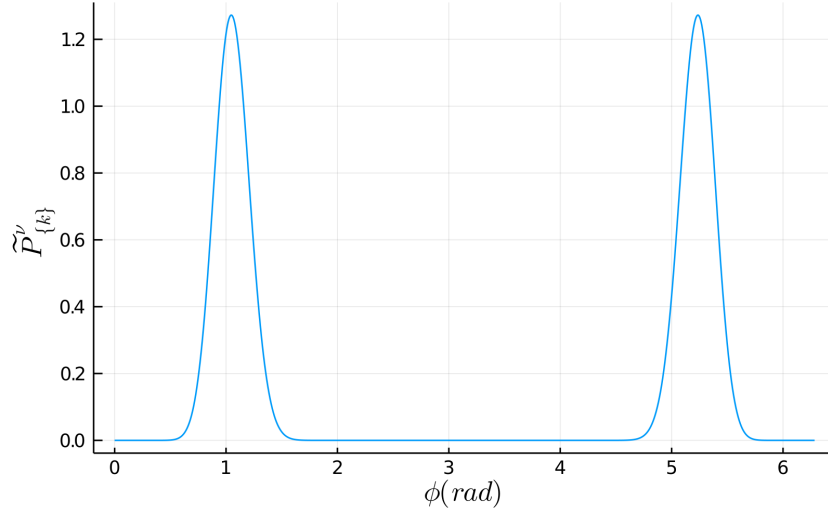
**Figure 2.1** Example of a possible probability distrubtion $\widetilde{P}^\nu_{\{k\}}(\phi)$ for a set of $\nu$ measurements $\{k\}$ generated using the methods described in Sec. 2.2.

distribution,

$$\widetilde{P}^\nu_{\{k\}} = \frac{1}{A} w(\phi) P^\nu_{\{k\}}(\phi, \nu, \{k\}). \tag{2.3}$$

The function $w(\phi)$ is a weight factor, allowing us to encode prior-known information about the probabilities of different values of the parameter $\phi$. For example, if all $\phi$ values are equally likely, then $w(\phi) = 1$. The variable $A$ is a normalization constant, and is defined by the equation

$$A = \int w(\phi) P^\nu_{\{k\}}(\phi, \nu, \{k\}) d\phi. \tag{2.4}$$

Plotting this function, $\widetilde{P}^\nu_{\{k\}}(\phi, \nu, \{k\})$, against the angle $\phi$ will give us some functional dependence, as seen in the example from Fig. 2.1.

We can draw a few conclusions from this plot. First, notice that there is an intrinsic width or range to the probe. It cannot distinguish between parameters $\phi = \pi - x$ and $\phi = \pi + x$, where $x \in [0, \pi]$. This range will differ for different systems and different probes, but it suffices to say that we need to restrict our analysis to the range of sensitivity of the probe. In this case, we will restrict

further analysis to the range $\phi \in [0, \pi]$. In this restricted range, we define $\phi_{mp}$, the most probable value of $\phi$ given the information we have. The quantity $\phi_{mp}$ is defined by the equation

$$\widetilde{P}^v_{\{k\}}(\phi_{mp}, v, \{k\}) = \max_{\phi} \left[ \widetilde{P}^v_{\{k\}}(\phi, v, \{k\}) \right]. \tag{2.5}$$

We can also define the probability that the parameter $\phi$ is between $a$ and $b$, with $a$ and $b$ in the domain of $\phi$:

$$P(a, b) = \int_a^b \widetilde{P}^v_{\{k\}}(\phi, v, \{k\}) d\phi. \tag{2.6}$$

Another useful value is the minimum length of the confidence interval $y$, defined as

$$L(CI)_y = \min_{a,b \in D(\phi)} (b - a), \tag{2.7}$$

such that

$$y = \int_a^b \widetilde{P}^v_{\{k\}}(\phi, v, \{k\}) d\phi. \tag{2.8}$$

The symbol $D(\phi)$ denotes the domain of $\phi$. Notice that while multiple confidence intervals are possible, this expression gives us the smallest length necessary to achieve a confidence of $y$.

There is one more important element to this framework. Each estimation has the potential to be different, due to the random nature of measurement. To compensate for this fact, we will simulate a large number of estimations, quantified in the variable $N_E$, with the same $v$ and initial probe state, then analyze four metrics from this set, which we define as $\mu(\phi_{mp}), \sigma(\phi_{mp}), \mu(L(CI)_{.95})$, and $\sigma(L(CI)_{.95})$. If $\phi_{mp,i}$ and $L(CI)_{.95,i}$ are the $\phi_{mp}$ and $L(CI)_{.95}$ estimated by the $i$th estimation in the set of $N_E$ estimations, then our metrics are defined as follows:

$$\mu(\phi_{mp}) = \frac{1}{N_E} \sum_i^{N_E} \phi_{mp,i} \tag{2.9}$$

$$\sigma(\phi_{mp}) = \frac{1}{N_E - 1} \sqrt{\sum_i^{N_E} (\phi_{mp,i} - \mu(\phi_{mp}))^2} \tag{2.10}$$

$$\mu(L(CI)_{.95}) = \frac{1}{N_E} \sum_i^{N_E} L(CI)_{.95,i} \tag{2.11}$$

$$\sigma(L(CI)_{.95}) = \frac{1}{N_E - 1} \sqrt{\sum_i^{N_E} (L(CI)_{.95,i} - \mu(L(CI)_{.95}))^2}. \tag{2.12}$$

The quantities $\mu(\phi_{mp})$ and $\sigma(\phi_{mp})$ are the mean and standard deviation of the $\phi_{mp}$ found by each estimation in the set, and $\mu(L(CI)_{.95})$ and $\sigma(L(CI)_{.95})$ are the mean and standard deviation of the length of the 95% confidence interval found by each estimation in the set. The 95% confidence interval was chosen somewhat arbitrarily as a value with good certainty, but not so high that it would always span the majority of the domain of $\phi$. In a nutshell, the parameters $\mu(\phi_{mp})$ and $\mu(L(CI)_{.95})$ encode the average accuracy and uncertainty of an estimation, and $\sigma(\phi_{mp})$ and $\sigma(L(CI)_{.95})$ encode how much variation there is in the accuracy and uncertainty between estimations. An ideal measurement set would find $\mu(\phi_{mp}) = \phi$, $\sigma(\phi_{mp}) = 0$, $\mu(L(CI)_{.95}) = 0$ and $\sigma(L(CI)_{.95}) = 0$. In practicality, the result $\phi_{mp}$ will vary wildly from one measurement to another, and will encode less useful information, so our analysis will use the metric $\mu(L(CI))$ as our uncertainty metric. The metric $\mu(L(CI))$ (as well as the other three metrics) are all dependent on the parameter $\phi$. We assume that we have no prior knowledge about the parameter $\phi$, so we are interested in reducing the uncertainty averaged over all possible angles $\phi$. We will denote this average using the notation $\text{mean}(\mu(L(CI)))$.

Now that we have defined an uncertainty metric appropriate for the regime of limited resources, we will formally introduce our two physical systems, a qubit measurement procedure and an interferometric measurement procedure, and calculate the uncertainty for each setup.

## 2.2 Qubit Metrology

A qubit is any quantum state in a 2-dimensional space. Examples include electron-spin states and two-level atoms. Unlike a classical bit, which only has two possible states, a qubit can exist in infinitely many different superpositions of its two basis states. In our measurement scheme, we will initialize qubit probes into a known state, then induce a rotation on the probes by an unknown angle $\phi$, and then estimate the angle of rotation using the methods described in the previous section.

In order to allow for entanglement within the probes, each probe will be comprised of two qubits. A single probe state, $|\psi\rangle$, will be represented as

$$|\psi\rangle = \alpha |\downarrow_1\downarrow_2\rangle + \beta |\downarrow_1\uparrow_2\rangle + \gamma|\uparrow_1\downarrow_2\rangle + \delta |\uparrow_1\uparrow_2\rangle = \begin{pmatrix} \alpha \\ \beta \\ \gamma \\ \delta \end{pmatrix}. \tag{2.13}$$

The state is normalized, so $|\alpha|^2 + |\beta|^2 + |\gamma|^2 + |\delta|^2 = 1$, and the subscripts 1 and 2 refer to the first and second qubit respectively, although they will be omitted in what follows. We are specifically interested in the effect of entanglement on the uncertainty of our measurement, so we will test initial probe states of the form

$$|\psi\rangle = \sqrt{\alpha} |\downarrow\uparrow\rangle + \sqrt{1-\alpha} |\uparrow\downarrow\rangle = \begin{pmatrix} 0 \\ \sqrt{\alpha} \\ \sqrt{1-\alpha} \\ 0 \end{pmatrix}, \tag{2.14}$$

where we have used the tensor-product representation of the two qubits. The parameter $\alpha$ will vary in the range $[0, 1/2]$, with $\alpha = 0$ corresponding to a separable, non-entangled state, and $\alpha = 1/2$ corresponding to the Bell state $|\Psi^+\rangle$, a maximally entangled state. The rotation $U_\phi$ will act independently on each qubit within the probe, and is expressed by the tensor-product matrix

$$U_\phi = \begin{pmatrix} \cos(\phi/2) & \sin(\phi/2) \\ -\sin(\phi/2) & \cos(\phi/2) \end{pmatrix} \otimes \begin{pmatrix} \cos(\phi/2) & \sin(\phi/2) \\ -\sin(\phi/2) & \cos(\phi/2) \end{pmatrix}. \tag{2.15}$$

An initial probe state $|\psi_i\rangle$ is evolved into the final probe state $|\psi_f\rangle$ by the formula

$$\left|\psi_f\right\rangle = U_\phi |\psi_i\rangle. \tag{2.16}$$

These states and evolutions which we have introduced have all been for pure quantum states not affected by noise. However, we are also interested in the effect of dephasing on our qubit

measurement procedure, and so will now generalize the previous formulae to include mixed, or noisy, quantum states as well. As the name suggests, a mixed quantum state $\rho$ can be thought of as a mixture of different pure quantum states, represented mathematically as

$$\rho = \sum_i p_i |\psi_i\rangle \langle \psi_i|. \tag{2.17}$$

The $|\psi_i\rangle$ are pure states, and the weight factor $p_i$ can be thought of as the probability that a mixed state $\rho$ will be measured in the state $|\psi_i\rangle$, although the expansion of a mixed state into a sum of pure states is not unique. To rotate an initial mixed state $\rho_i$ by an angle $\phi$, the formula becomes

$$\rho_f = U_\phi \rho_i U_\phi^\dagger, \tag{2.18}$$

where the rotation matrix $U_\phi$ is unchanged from the pure state case.

The function $\Xi_i(\phi)$, as introduced in Sec. 2.1.2 and from which we can calculate the $L(CI)$ for a measurement, is

$$\Xi_i(\phi) = |\langle \xi_i| U_\phi |\psi\rangle|^2 = \text{Tr}\left(|\xi_i\rangle \langle \xi_i| U_\phi \rho U_\phi^\dagger\right). \tag{2.19}$$

The possible measurement states $|\xi_i\rangle$ are $|\downarrow\downarrow\rangle, |\downarrow\uparrow\rangle, |\uparrow\downarrow\rangle$, and $|\uparrow\uparrow\rangle$.

The last piece we need is how we will implement dephasing noise in our qubit measurement procedure. Dephasing, which reduces the coherence of a quantum system, decreases the amplitude of the off-diagonal elements of the state's density matrix, transforming a single qubit state $\rho_i$ into $\rho_f$ as shown,

$$\rho_i = \begin{pmatrix} \rho_{11} & \rho_{12} \\ \rho_{21} & \rho_{22} \end{pmatrix} \rightarrow \rho_f = \begin{pmatrix} \rho_{11} & \sqrt{\eta}\rho_{12} \\ \sqrt{\eta}\rho_{21} & \rho_{22} \end{pmatrix}. \tag{2.20}$$

The parameter $\eta$ describes how strong the dephasing noise is: $\eta = 1$ corresponds to no dephasing, and $\eta = 0$ corresponds to total dephasing. Dephasing is implemented on a single qubit via the

formula [7]

$$\rho_f = K_0 \rho_i K_0^\dagger + K_1 \rho_i K_1^\dagger = \begin{pmatrix} \rho_{11} & \sqrt{\eta}\,\rho_{12} \\ \sqrt{\eta}\,\rho_{21} & \rho_{22} \end{pmatrix}. \tag{2.21}$$

where the operators $K_0$ and $K_1$ are two different transformations, defined as

$$K_0 = \left( \frac{1 + \sqrt{\eta}}{2} \right)^{1/2} \begin{pmatrix} 1 & 0 \\ 0 & 1 \end{pmatrix} \tag{2.22}$$

$$K_1 = \left( \frac{1 - \sqrt{\eta}}{2} \right)^{1/2} \begin{pmatrix} 1 & 0 \\ 0 & -1 \end{pmatrix}, \tag{2.23}$$

and the dagger represents the Hermitian conjugate. Implementing dephasing on two qubits is done by taking the tensor product of two noisy single qubits, resulting in the formula

$$\rho_f = \sum_{i,j=0,1} K_i \otimes K_j \rho_i K_i^\dagger \otimes K_j^\dagger. \tag{2.24}$$

Due to computational constraints, we need to implement the noise discretely in our simulations. To add noise in $n$ steps, we'll first add noise, then rotate by the angle $\phi/n$, then repeat $n$ times. We can name the operator for a single noisy rotation $\Lambda$, where

$$\Lambda = \sum_{i,j=0,1} U_{\phi/n} \left( K_i \otimes K_j \right). \tag{2.25}$$

A full rotation would have the form

$$\rho_f = \left( \prod_{m=1}^{n} \Lambda \right) \rho_i \left( \prod_{m=1}^{n} \Lambda^\dagger \right). \tag{2.26}$$

This gives us all the tools necessary to allow us to simulate both noiseless and noisy two-qubit probes being rotated by an angle $\phi$, and then to measure the probes and estimate the parameter $\phi$.

**Figure 2.2** Diagram of a Mach-Zehnder Interferometer.

## 2.3 Interferometric Metrology

The second setup we will study is the Mach-Zehnder interferometer (MZI), as shown in Fig. (2.2). The MZI mixes two beams, labeled 0 and 1 in the figure, using a beam splitter. A phase shift is implemented on one of the MZI arms post-mixing, and the two beams are again mixed using a second beam splitter. The phase shift can be detected by measuring the two output beams, labeled 4 and 5 in the figure.

We will analyze two different input beams: the number state and the coherent state. The number state, written $|n\rangle$, is a non-classical state of light which contains exactly $n$ photons. The coherent state, written $|\alpha\rangle$, is the most-classical state of light and contains an average of $\alpha$ photons. We can express both these states in terms of creation $\hat{a}^\dagger$ and annihilation $\hat{a}$ operators, which, similar to the quantum simple harmonic oscillator creation and annihilation operators, represent adding and

removing photons from the light. These two states of light are written

$$|n\rangle = \frac{1}{\sqrt{n!}} \left(\hat{a}^\dagger\right)^n |0\rangle, \tag{2.27}$$

$$|\alpha\rangle = \exp\left[\alpha\hat{a}^\dagger - \alpha^*\hat{a}\right] |0\rangle. \tag{2.28}$$

The state $|0\rangle$ denotes the vacuum state. These two forms will be useful when propagating these states through the MZI.

Now, in order to find the possible measurement outputs for each input state, and then to calculate the uncertainty, we will propagate both of these states through the MZI. The MZI has three components we need to model: the initial beam splitter, the phase shift, then the final beam splitter. As explained in [10], we can describe each of these components by how they transform the annihilation and creation operators. In our notation, $\hat{a}_i$ denotes the annihilation operator for the state on the $i$th beam. The key connection here is that the vacuum on either side of these elements remains unchanged, so if we can express a state in terms of only creation/annihilation operators and the vacuum, then to propagate the state across one of these three elements we would transform the operators by these rules and leave the vacuum unchanged. The transformation rules, labeled by the element they are describing, are

$$\hat{a}_0 \xrightarrow{\text{BS1}} \frac{1}{\sqrt{2}}(\hat{a}_2 - i\hat{a}_3) \tag{2.29}$$

$$\hat{a}_1 \xrightarrow{\text{BS1}} \frac{1}{\sqrt{2}}(-i\hat{a}_2 + \hat{a}_3) \tag{2.30}$$

$$\hat{a}_2 \xrightarrow{\phi} e^{i\phi}\hat{a}_2 \tag{2.31}$$

$$\hat{a}_3 \xrightarrow{\text{BS2}} \frac{1}{\sqrt{2}}(\hat{a}_4 - i\hat{a}_5) \tag{2.32}$$

$$\hat{a}_2 \xrightarrow{\text{BS2}} \frac{1}{\sqrt{2}}(-i\hat{a}_4 + \hat{a}_5). \tag{2.33}$$

One last note: the MZI requires two inputs, so we will pair both of the states of interest, the number state and the coherent state, with the vacuum state. This is equivalent to leaving the second port of

the MZI untouched. With these tools we are now ready to propagate the number and coherent states

through the MZI. We begin with the coherent input:

$$|0\,\alpha\rangle_{01} = \frac{1}{\sqrt{2}} \left( \exp[\alpha\hat{a}_1^\dagger - \alpha^*\hat{a}_1] \,|00\rangle_{01} \right) \tag{2.34}$$

$$\xrightarrow{\text{BS1}} \frac{1}{\sqrt{2}} \left( \exp\left[ \frac{i\alpha}{\sqrt{2}}\hat{a}_2^\dagger - \frac{(-i)\alpha^*}{\sqrt{2}}\hat{a}_2 \right] \exp\left[ \frac{\alpha}{\sqrt{2}}\hat{a}_3^\dagger - \frac{\alpha^*}{\sqrt{2}}\hat{a}_3 \right] |00\rangle_{23} \right) \tag{2.35}$$

$$\xrightarrow{\phi} \frac{1}{\sqrt{2}} \left( \exp\left[ \frac{i\alpha}{\sqrt{2}}e^{i\phi}\hat{a}_2^\dagger - \frac{(-i)\alpha^*}{\sqrt{2}}e^{i\phi}\hat{a}_2 \right] \exp\left[ \frac{\alpha}{\sqrt{2}}\hat{a}_3^\dagger - \frac{\alpha^*}{\sqrt{2}}\hat{a}_3 \right] |00\rangle_{23} \right) \tag{2.36}$$

$$\xrightarrow{\text{BS2}} \frac{1}{\sqrt{2}} \left( \exp\left[ \frac{\alpha}{2}\left(1 - e^{i\theta}\right)\hat{a}_4^\dagger - \frac{\alpha^*}{2}\left(1 - e^{-i\theta}\right)\hat{a}_4 \right] \right.$$

$$\left. \exp\left[ \frac{i\alpha}{2}\left(1 + e^{i\theta}\right)\hat{a}_5^\dagger - \frac{(-i)\alpha^*}{2}\left(1 + e^{-i\theta}\right)\hat{a}_5 \right] |00\rangle_{45} \right)$$

$$U_\phi(\phi)\,|0\,\alpha\rangle_{01} = \frac{1}{\sqrt{2}} \left| \frac{\alpha(1 - e^{i\theta})}{2} \right\rangle_4 \left| \frac{i\alpha(1 + e^{i\theta})}{2} \right\rangle_5 \tag{2.37}$$

$$= e^{-\frac{1}{2}\left| \frac{\alpha(1-e^{i\phi})}{2} \right|^2} e^{-\frac{1}{2}\left| \frac{i\alpha(1+e^{i\phi})}{2} \right|^2} \sum_{m,n}^\infty \frac{1}{\sqrt{m!n!}} \left( \frac{\alpha\left(1 - e^{i\phi}\right)}{2} \right)^m \left( \frac{i\alpha\left(1 + e^{i\phi}\right)}{2} \right)^n |m\rangle_4\,|n\rangle_5.$$

$$\tag{2.38}$$

We express the final output state, denoted $U_\phi(\phi)\,|0\alpha\rangle_{01}$, in terms of number states, because our

detectors will read in a specific number of photons. We now compute the output for the number

input:

$$|0\,n\rangle_0 1 = \frac{1}{\sqrt{n!}}\left(\hat{a}_1^\dagger\right)^n |00\rangle_{01} \tag{2.39}$$

$$\xrightarrow{\text{BS1}} \frac{1}{\sqrt{n!}}\left(\frac{1}{\sqrt{2}}\left(i\hat{a}_2^\dagger + \hat{a}_3^\dagger\right)\right)^n |00\rangle_{23} \tag{2.40}$$

$$\xrightarrow{\text{BS2}} \frac{1}{\sqrt{n!}}\left(\frac{1}{2}\left(ie^{i\phi}\hat{a}_2^\dagger + \hat{a}_3^\dagger\right)\right)^n |00\rangle_{23} \tag{2.41}$$

$$\xrightarrow{\phi} \frac{1}{\sqrt{n!}}\left(\frac{1}{\sqrt{2}}\left(\left(1-e^{i\phi}\right)\hat{a}_4^\dagger + i\left(1+e^{i\phi}\right)\hat{a}_5^\dagger\right)\right)^n |00\rangle_{45} \tag{2.42}$$

$$U_\phi(\phi)|0\,n\rangle_{01} = \frac{1}{2^n\sqrt{n!}}\sum_{k=0}^n \binom{n}{k}\sqrt{(n-k)!}\left(1-e^{i\phi}\right)^{n-k}\sqrt{k!}\left(i\left(1+e^{i\phi}\right)\right)^k |n-k\rangle_4 |k\rangle_5. \tag{2.43}$$

Knowing the output states for both inputs, we can find the probability of measuring an output $|m\,n\rangle$, corresponding to the function $\Xi_i(\phi)$ derived in Sec. (2.1):

$$\Xi(\phi)_{mn}^{(\alpha)} = \left|\langle m\,n| U_\phi(\phi) |0\,\alpha\rangle\right|^2 = \left| \frac{e^{-\frac{1}{2}\left|\frac{\alpha(1-e^{i\phi})}{2}\right|^2} e^{-\frac{1}{2}\left|\frac{i\alpha(1+e^{i\phi})}{2}\right|^2}}{\sqrt{m!n!}}\left(\frac{\alpha\left(1-e^{i\phi}\right)}{2}\right)^m \left(\frac{i\alpha\left(1+e^{i\phi}\right)}{2}\right)^n \right|^2 \tag{2.44}$$

$$\Xi(\phi)_{mn}^{(n)} = \left|\langle m\,n| U_\phi(\phi) |0\,n\rangle\right|^2 = \left| \frac{\sqrt{(n-k)!}\sqrt{k!}}{2^n\sqrt{n!}}\binom{n}{k}\left(1-e^{i\phi}\right)^{n-k}\left(i\left(1+e^{i\phi}\right)\right)^k \right|^2. \tag{2.45}$$

From these two equations, we can follow the steps in Sec. (2.1) to determine the uncertainty given a specific set of measurement results.

## 2.4   Computational Considerations

We will be using simulations to study both noiseless and noisy measurement procedures, so it is in order to note a few computational considerations. First, quantum measurement is inherently

random. In order to simulate that randomness, we will use a random number generator to determine the output of each measurement, with outcomes weighted by their probabilities. The consequence of this method is that each simulation will be slightly different. To account for this fact, we will run multiple trials of each simulation and study the average behavior of the trials, as described in Sec. 2.1.2.

Second, we will need to sample a large number of values of $\phi$ to determine the confidence interval $L(CI)$. We can use Monte-Carlo methods to determine this quantity. We will begin by randomly sampling the entire domain of $\phi$, then estimating $L(CI)$. If $L(CI)$ is outside a certain error tolerance, we focus in on areas of interest, then sample additional angles $\phi$ within those regions in order to accurately compute the uncertainty. In doing so, we need to determine the accuracy tolerance for our uncertainty. Once the uncertainty is changing less than a threshold value of $\tau$, we stop sampling additional points. In our simulations we will set this threshold to $\tau = 10^{-3}$ rad.

Third, we discretely compute the uncertainty averaged over all angles $\phi$, $\mathrm{mean}(\mu(L(CI)))$. To ensure consistency in our averages, we averaged over $N_\phi$ angles evenly spaced between 0 and $\pi/2$. For the noiseless simulations, we used $N_\phi = 20$, and for the noisy simulations, we used $N_\phi = 10$.

Finally, we repeated each estimation $N_E$ times, as described in Sec. 2.1.2. For the noiseless simulations, we used $N_E = 10^3$, and for the noisy simulations we used $N_E = 5 \cdot 10^2$.

Due to computational constraints, the values of $N_\phi$ and $N_E$ are lower for the noisy simulations, reducing the number of points we will average over in the noisy datasets. We tested various values of $N_\phi$ and $N_E$ in the noiseless simulations, and found that decreasing either value make the resulting plots less smooth, but as long as both values were above a certain threshold, $N_\phi \gtrsim 5$ and $N_E \gtrsim 100$, the plots did not change qualitatively. As such, the reduced values of $N_\phi$ and $N_E$ in the noisy simulations will limit the precision to which we can make statements about the effect of noise on our probes, but we do not believe that they will qualitatively alter our results.

In this chapter, we have derived the necessary equations and tools to propagate probes through

both our qubit measurement procedure and the MZI, and have a reasonable method of quantifying the uncertainty of our estimations. We have also considered some important computational considerations for our simulations. Results for the qubit measurement procedure simulations are presented in Chapter 3. Preliminary results for the MZI simulations are given in Appendix A.

# Chapter 3

# Results

In this section we present the results of our qubit metrology scheme simulations. We use our simulations to compute the uncertainty metric $\text{mean}(\mu(L(CI)))$ for the qubit estimation procedure, as described in Sec. 2.4. We perform our simulations using three different levels of dephasing noise: noiseless ($\eta = 1.0$), low noise ($\eta = 0.9$), and high noise ($\eta = 0.5$). These regimes are qualitatively labeled. We find that in the low noise regime, the quantum advantage is reduced, and in the high noise regime, that advantage is lost all together.

## 3.1 Noiseless Qubit Quantum Metrology Results

Our results for the noiseless qubit measurement simulation are given in Figs. 3.1 and 3.2. We tested the initial probe state $|\psi\rangle = \sqrt{\alpha}\,|\!\downarrow\uparrow\rangle + \sqrt{1-\alpha}\,|\!\uparrow\downarrow\rangle$ for four different values of $\alpha$: 0, 1/6, 1/3, and 1/2. When $\alpha = 0$, the probe is separable, and when $\alpha = 1/2$, the probe is a maximally entangled Bell state. The closer $\alpha$ is to 1/2, the more entangled the probe is [11]. Figure 3.1 gives the uncertainty for each state as a function of $\nu$, the number of probes used in the measurement. Figure 3.2 gives the relative uncertainty for the three entangled probe states, defined as the uncertainty of the entangled probe divided by the uncertainty of the separable probe for the same number of
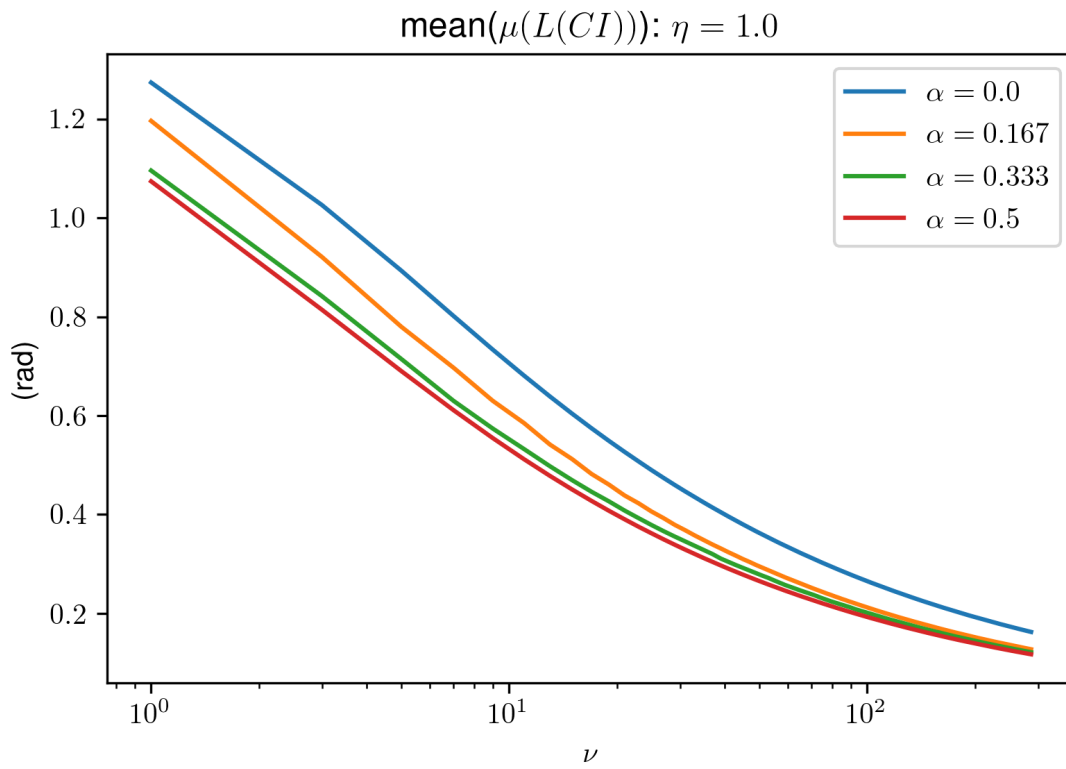
**Figure 3.1** The uncertainty from our noiseless simulation ($\eta = 1.0$) as a function of the number of measurements $\nu$, shown for four different initial states parameterized by $\alpha$, $|\psi\rangle = \sqrt{\alpha}\,|\!\downarrow\uparrow\rangle + \sqrt{1-\alpha}\,|\!\uparrow\downarrow\rangle$.
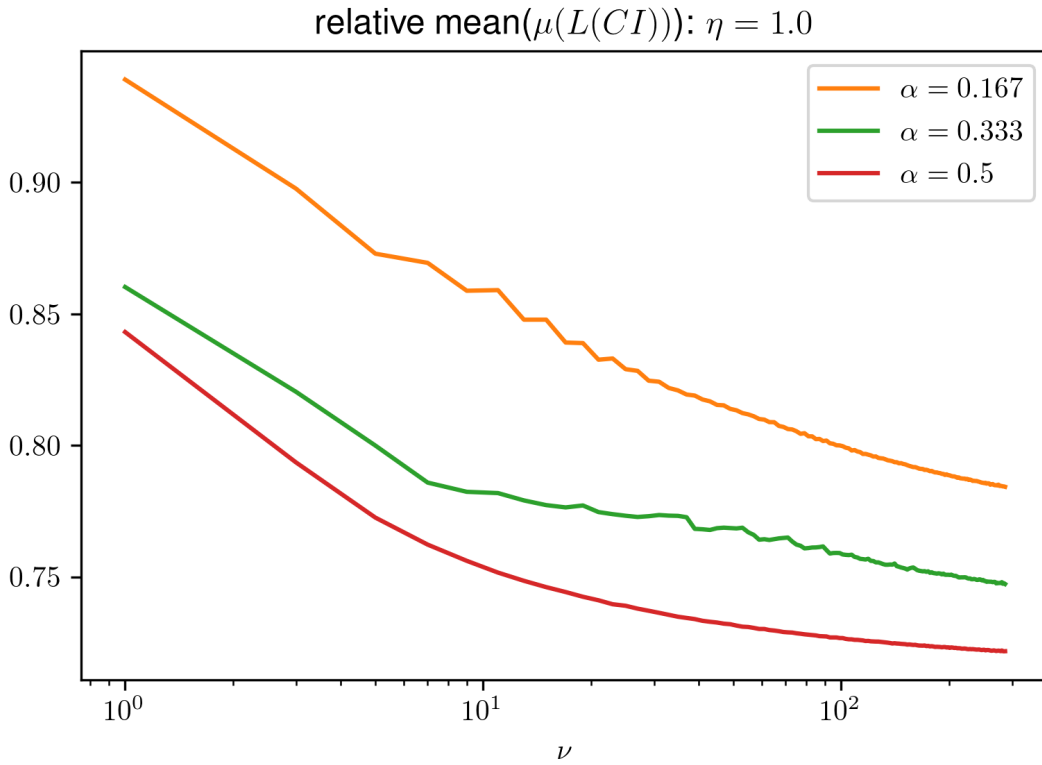
**Figure 3.2** The relative uncertainty from our noiseless simulation ($\eta = 1.0$) as a function of the number of measurements $\nu$, shown for three different initial states parameterized by $\alpha$, $|\psi\rangle = \sqrt{\alpha}\,|\downarrow\uparrow\rangle + \sqrt{1-\alpha}\,|\uparrow\downarrow\rangle$. The relative uncertainty is the ratio between the uncertainty of a given initial state $|\psi\rangle$ and the uncertainty of the separable state $|\psi\rangle = |\downarrow\uparrow\rangle$, both for the same number of measurements $\nu$.

probes $v$. This relative uncertainty allows us to see if the entangled probe state is performing better (relative uncertainty less than one) or worse (relative uncertainty greater than one) than the separable probe state.

Equation (1.2) from Sec. 1.2 tells us that as the number of measurements $v$ becomes asymptotically large, the relative uncertainty for the maximally entangled state should approach $1/\sqrt{2} \approx 0.71$. We are using our own uncertainty metric, but this claim still seems to hold: Fig. 3.1 shows that the relative uncertainty for the state $\alpha = 0.5$ seems to be approaching an asymptote in the region of 0.71, although we have insufficient data to state this conclusively. However, as the number of measurements $v$ decreases, the relative uncertainty also decreases. Apparently, the advantage of using the entangled states decreases as the number of probes $v$ decreases. A single maximally entangled probe gives an uncertainty about 15% smaller than a single separable probe, but ten maximally entangled probes give an uncertainty about 25% smaller than ten separable probes.

## 3.2   Noisy Qubit Quantum Metrology Results

In this section, we consider the effect of dephasing noise on the qubit estimation procedure. We use the procedure described by Eq. (2.26). The noise is implemented in $n = 5$ discrete steps and is parameterized by $\eta$. If $\eta = 1.0$, then there is no dephasing, and if $\eta = 0$, there is total dephasing. We simulate two cases: low noise ($\eta = 0.9$), and high noise ($\eta = 0.5$).

Our results are given for the two cases in Figs. 3.3–3.6. Figures 3.3 and 3.5 show the results in absolute form, and Figs. 3.4 and 3.6 show the results in relative form (where the ratio between the uncertainty of the entangled state and the separable state is plotted).

We consider first the low noise case. Figure 3.3 shows that, for all four values of $\alpha$, increasing the number of measurements $v$ decreases the uncertainty of the estimation. Additionally, Fig. 3.4 shows that for all values of $v$ plotted, the entangled states outperform the separable state. For low $v$,
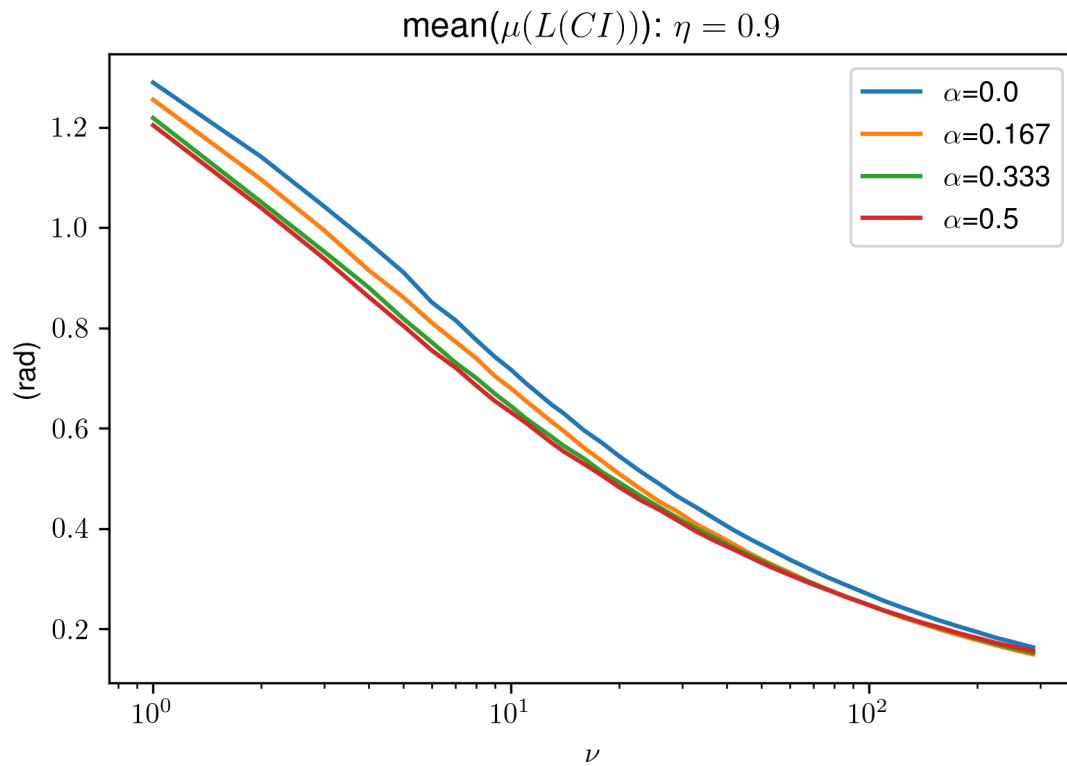
**Figure 3.3** The uncertainty from our low noise simulation ($\eta = 0.9$) as a function of the number of measurements $\nu$, shown for four different initial states parameterized by $\alpha$, $|\psi\rangle = \sqrt{\alpha}\,|\downarrow\uparrow\rangle + \sqrt{1-\alpha}\,|\uparrow\downarrow\rangle$.
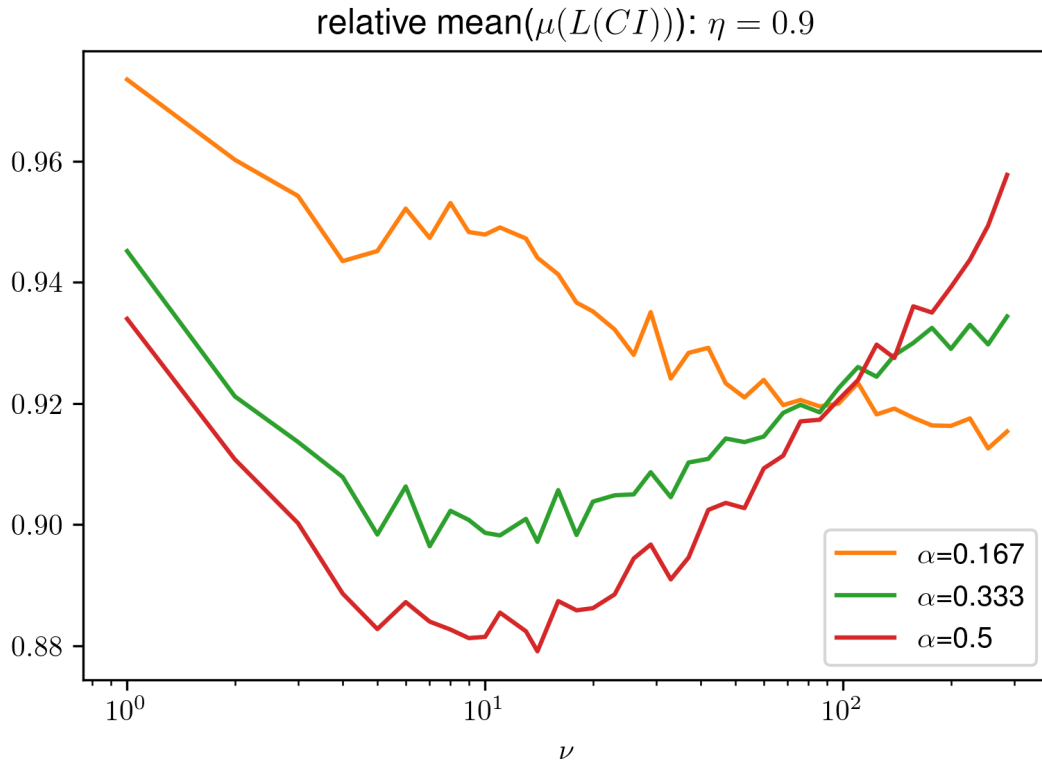
**Figure 3.4** The relative uncertainty from our low noise simulation ($\eta = 0.9$) as a function of the number of measurements $\nu$, shown for three different initial states parameterized by $\alpha$, $|\psi\rangle = \sqrt{\alpha}\,|\downarrow\uparrow\rangle + \sqrt{1-\alpha}\,|\uparrow\downarrow\rangle$. The relative uncertainty is the ratio between the uncertainty of a given initial state $|\psi\rangle$ and the uncertainty of the separable state $|\psi\rangle = |\downarrow\uparrow\rangle$, both for the same number of measurements $\nu$.
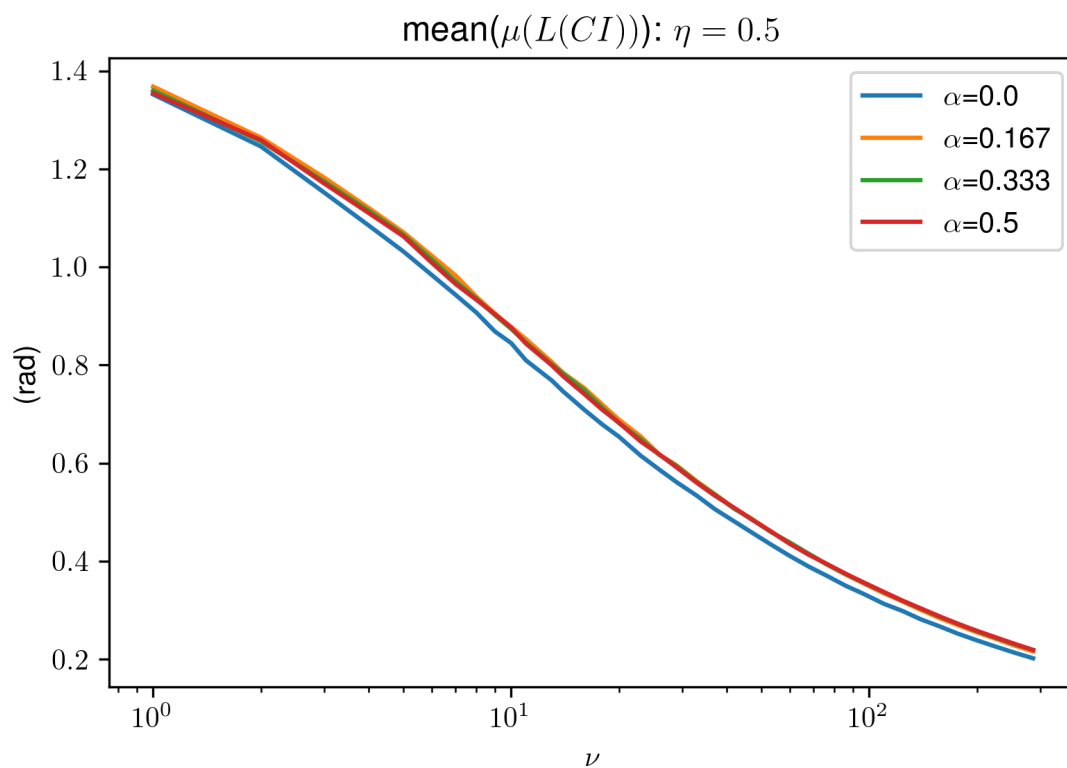
**Figure 3.5** The uncertainty from our high noise simulation ($\eta = 0.5$) as a function of the number of measurements $\nu$, shown for four different initial states parameterized by $\alpha$, $|\psi\rangle = \sqrt{\alpha}\,|\downarrow\uparrow\rangle + \sqrt{1-\alpha}\,|\uparrow\downarrow\rangle$.
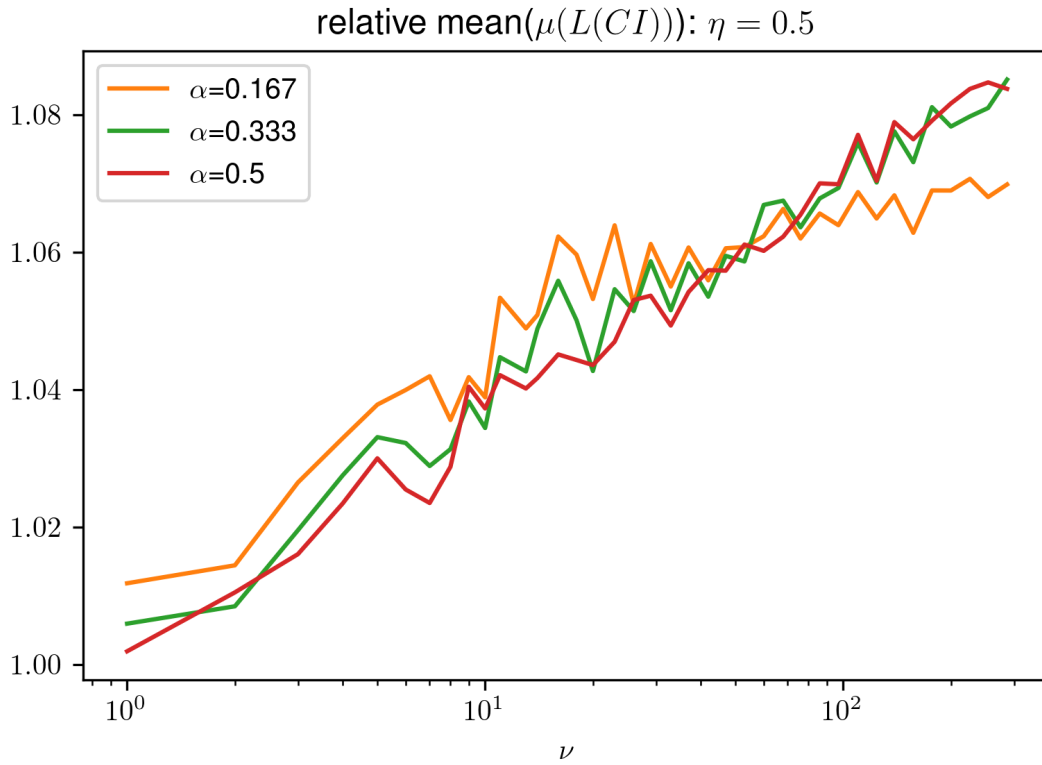
**Figure 3.6** The relative uncertainty from our high noise simulation ($\eta = 0.5$) as a function of the number of measurements $\nu$, shown for three different initial states parameterized by $\alpha$, $|\psi\rangle = \sqrt{\alpha}\,|\downarrow\uparrow\rangle + \sqrt{1-\alpha}\,|\uparrow\downarrow\rangle$. The relative uncertainty is the ratio between the uncertainty of a given initial state $|\psi\rangle$ and the uncertainty of the separable state $|\psi\rangle = |\downarrow\uparrow\rangle$, both for the same number of measurements $\nu$.

the more entangled a state is, the better it outperforms the separable state.

Notice, however, that in comparison to the noiseless simulation in Fig. 3.2, the quantum advantage is smaller in the noisy simulation–the relative uncertainty for the maximally entangled state at $\nu = 10$ is equal to approximately 0.88 for the noisy simulation, whereas it was equal to about 0.75 for the noiseless simulation.

Furthermore, as $\nu$ increases, the less entangled states gradually outperform the maximally entangled state, and the relative uncertainty for $\alpha = 0.5$ and $\alpha = 0.333$ seem to be trending towards 1.0. We expect that if a wider range of $\nu$ values were plotted, we would see the same behavior for the $\alpha = 0.167$ state as well.

In the case of high noise, Fig. 3.5 shows that the uncertainty of the estimation decreases as the number of measurements $\nu$ increases for all four values of $\alpha$. Notice, though, that the relative plot in Fig. 3.6 shows that the relative uncertainty is greater than one for all values of $\nu$. Not only is there no quantum advantage, but there even seems to be a quantum disadvantage. Within the accuracy of our simulation, there doesn't seem to be a definitive difference between the three entangled states, although the state $\alpha = 0.167$ does seem to outperform the other two at large enough $\nu$ values.

In summary, both of our noisy simulations showed that the uncertainty of the estimation decreases as the number of measurements increases, regardless of the probe state used. With regards to the quantum advantage, our low noise simulations indicate that it does still exist, although it is smaller than in the noiseless case. As $\nu$ increases, less entangled states begin to outperform the maximally entangled state, and the quantum advantage appears to vanish all together as $\nu$ becomes sufficiently large.

In the case of high noise, there is no quantum advantage for any value of $\nu$, and in fact there appears to be a quantum disadvantage. Our simulations indicate no clear distinction between the three entangled states in the presence of high noise.

It is worth reiterating that our model added dephasing in five discrete steps. In a physical

experiment, we would expect noise to affect the probes continuously, so further work would be in order to determine which of these features hold as noise is added to the probes in smaller increments.

## 3.3   Conclusion

Quantum metrology shows how quantum resources, such as entanglement, can decrease the uncertainty of a parameter estimation. If asymptotically many measurement resources are available, then this phenomenon is well described by the Quantum Cramer-Rao Bound [1]. However, there is no general description of the quantum advantage in the regime of limited measurement resources.

We have defined an Bayesian uncertainty quantifier appropriate to this regime of limited resources, and developed the mathematical description necessary to simulate both our qubit estimation scheme and the Mach-Zehnder interferometer estimation scheme. We then used simulations to study qubit probes measuring a rotation angle $\phi$. We simulated both noiseless and noisy estimation schemes. Our noiseless results show that, for the class of states we tested, entanglement always decreases the uncertainty of a measurement procedure, although the quantum advantage is reduced when fewer probes are used. Our noisy results, on the other hand, show that for small amounts of dephasing noise, the entangled states outperformed the separable state up to a given number of measurements $\nu$, after which point the separable state outperformed the entangled states. In the presence of large amounts of dephasing noise, the separable state outperforms the entangled states for all values of $\nu$.

It is important to note that our results are not general. We tested a specific class of states, $|\psi\rangle = \sqrt{\alpha}\,|{\downarrow}{\uparrow}\rangle + \sqrt{1-\alpha}\,|{\uparrow}{\downarrow}\rangle$, and our conclusions apply only to that class of states. We have performed preliminary work that indicates that our class of states is representative of a larger space of quantum states, but further work needs to be done to extend these conclusions to all qubit states.

# Appendix A

# Preliminary Results from the Mach-Zehnder Interferometer Simulations

As described in Sec. 2.3, we simulated two different states of light within the Mach-Zehnder interferometer: the number state, which is a non-classical state of light, and the coherent state, which is the most classical-like state of light. The number state is described by the number of photons, $n$, and the coherent state is described by the average number of photons, $\alpha$. When comparing the two states of light, we set $n = \alpha = p$, where $p$ corresponds to the number of photons in the number state and the average number of photons in the coherent state. We present preliminary results for the absolute uncertainty for $p = 1, 5$, and $10$ in Figs. A.1–A.3, and the relative uncertainty for each value in Fig. A.4.

When considering Figs. A.1–A.3, notice that as $p$ increases, the uncertainty for both number and coherent states decrease for all values of $v$. This result matches our expectations, as increasing $p$ is roughly analogous to increasing the number of probes. Increasing $p$ and increasing $v$ are, however, different operations and appear to lead to qualitatively different results, as can be seen by comparing the ordering of the coherent states at $p = 1, v = 10$ (an interpolated point), and $p = 10, v = 1$.
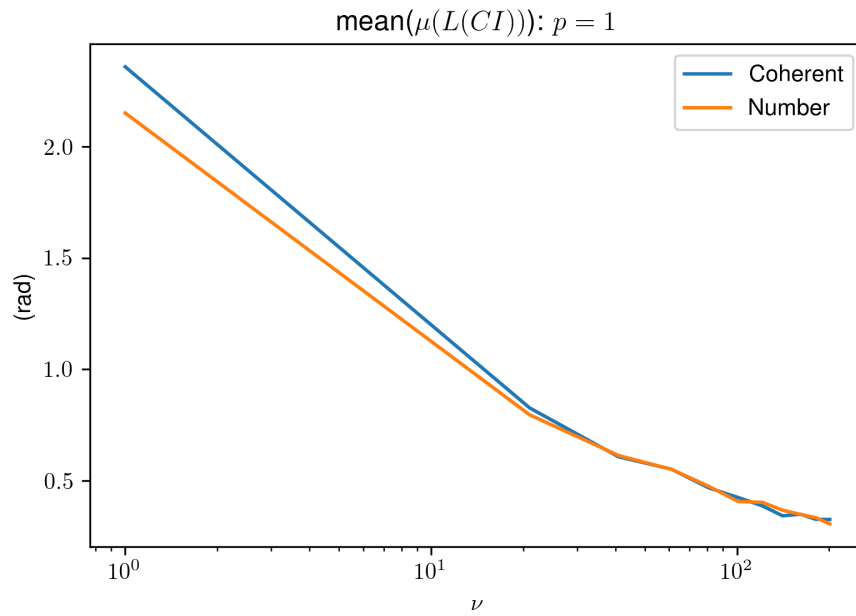
**Figure A.1** test 1
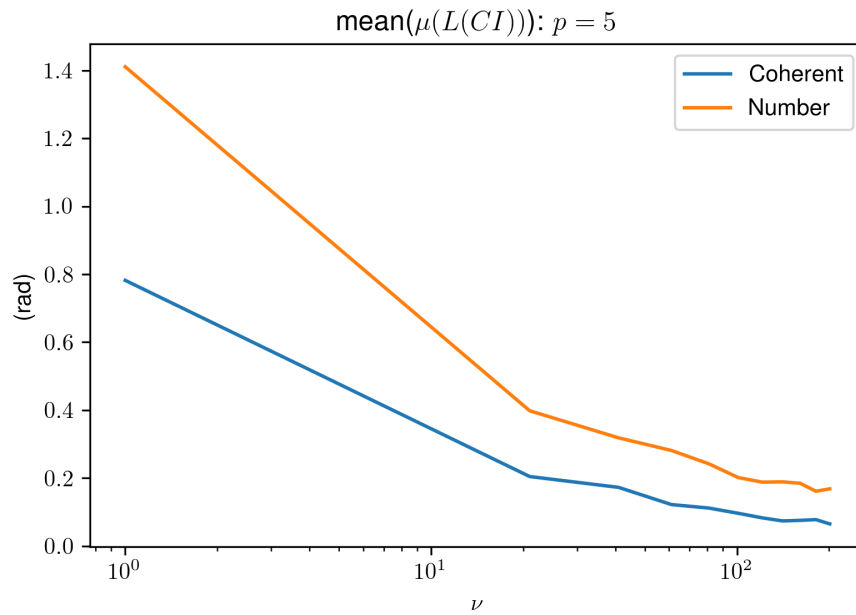


**Figure A.2** test 5
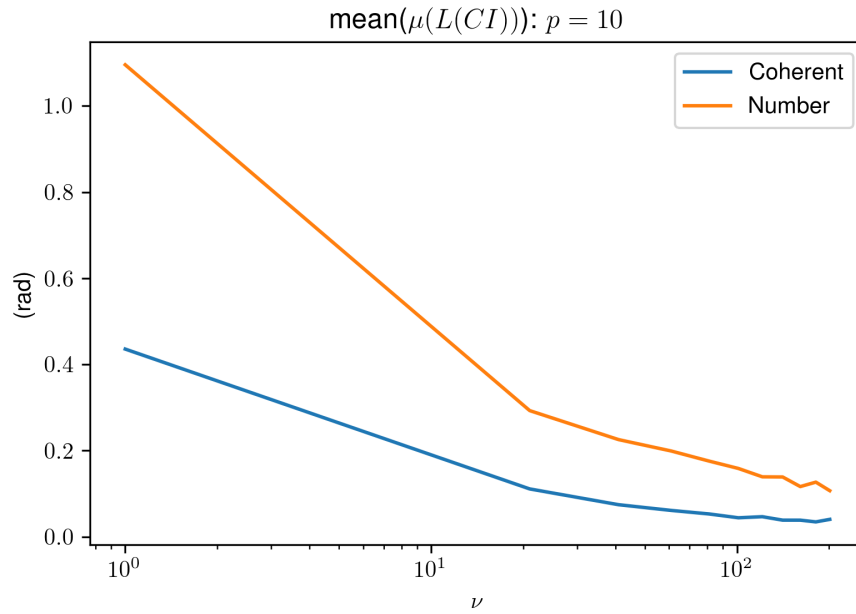
**Figure A.3** test 10
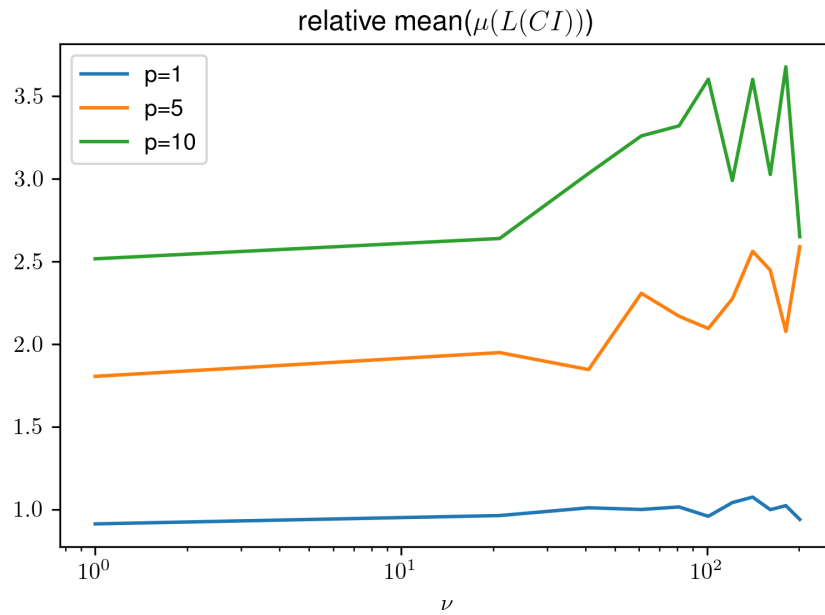


**Figure A.4**

Although the total number of photons utilized at each point is identical, when $p = 1$, the number state has a lower uncertainty than the coherent state, and when $p = 10$, the coherent state instead has a lower uncertainty than the number state.

Figure A.4 plots the relative uncertainty as a function of $v$ for each of the three $p$ values. In this plot, the relative uncertainty is defined as the uncertainty from the number state for a given $p$ value, divided by the uncertainty from the coherent state for the same value. Thus each line in the plot is the ratio of two unique datasets, with both datasets corresponding to the same $p$ value. When $p = 1$, the uncertainties from the coherent and the number states are nearly identical within the range of $v$ plotted. As $p$ increases, the relative uncertainty increases to a factor of two and then three, meaning that the uncertainty from the number state is that much larger than the uncertainty from the coherent state. There is insufficient data to determine if the relative uncertainty is approaching some limit as $p$ increases, and the numerical fluctuations in the plot are too large to determine whether the relative uncertainty for each value is changing with $v$ or staying constant.

This data indicates that using a number state to estimate the phase shift within the Mach-Zehnder interferometer leads to a larger uncertainty than using a coherent state. This is despite the fact that the coherent state is a classical-like state of light, while the number state is very non-classical. This is the opposite of what was found from the qubit estimation scheme, where increasing the non-classicality of the states, there manifest as entanglement, decreased the uncertainty of the estimation.

These results are preliminary: further simulation and study is required to either confirm or refute them.

# Bibliography

[1] S. L. Braunstein and C. M. Caves, "Statistical distance and the geometry of quantum states," Phys. Rev. Lett. **72,** 3439–3443 (1994).

[2] H. Cramér, in *Mathematical methods of statistics* (Princeton University Press, 1946), p. 500.

[3] V. Giovannetti, S. Lloyd, and L. Maccone, "Quantum metrology," Phys. Rev. Lett. **96,** 010401 (2006).

[4] M. Tsang, "Ziv-Zakai error bounds for quantum parameter estimation," Phys. Rev. Lett. **108,** 230401 (2012).

[5] X.-M. Lu and M. Tsang, "Quantum Weiss-Weinstein bounds for quantum metrology," Quantum Science and Technology **1,** 015002 (2016).

[6] J. Rubio, Ph.D. thesis, University of Sussex, 2019.

[7] R. Demkowicz-Dobrzański and L. Maccone, "Using entanglement against noise in quantum metrology," Phys. Rev. Lett. **113,** 250801 (2014).

[8] R. Nichols, T. R. Bromley, L. A. Correa, and G. Adesso, "Practical quantum metrology in noisy environments," Phys. Rev. A **94,** 042101 (2016).

[9] R. Demkowicz-Dobrzański, W. Górecki, and M. Guţă, "Multi-parameter estimation beyond quantum Fisher information," Journal of Physics A: Mathematical and Theoretical **53,** 363001 (2020).

[10] C. Gerry and P. Knight, in *Introductory quantum optics* (Cambridge University Press, 2004), Chap. 6,  pp. 137–143.

[11] R. Horodecki, P. Horodecki, M. Horodecki, and K. Horodecki, "Quantum entanglement," Rev. Mod. Phys. **81,** 912 (2009).

# Index